

# Power Quality Improvement in EV Charging Station Using PV-Based Shunt Active Power Filter

Pratik Potdukhe<sup>1</sup>, Praful Tadse<sup>2</sup>

<sup>1</sup> M.Tech Scholar, Dept. of Electrical Engineering, BIT Ballarpur Institute of Technology, Maharashtra, India

<sup>2</sup> Professor, Dept. of Electrical Engineering, BIT Ballarpur Institute of Technology, Maharashtra, India

\*\*\*

**Abstract** -The rapid proliferation of electric vehicle (EV) charging infrastructure has introduced significant power quality challenges in distribution systems due to the nonlinear nature of EV chargers. These chargers, typically implemented using three-phase diode bridge rectifiers, draw non-sinusoidal currents from the grid, resulting in high Total Harmonic Distortion (THD), reduced power factor, and increased system losses.

This paper presents the design and simulation of a photovoltaic (PV)-integrated Shunt Active Power Filter (SAPF) for harmonic mitigation in grid-connected EV charging stations. The system models three EV charging units, where two operate under steady-state conditions and one represents a dynamic load with time-varying connection to emulate real-world charging behavior. A 4 kW PV array is integrated with the SAPF DC link through a boost converter controlled using a Perturb and Observe (P&O) Maximum Power Point Tracking (MPPT) algorithm.

The Synchronous Reference Frame (SRF) control strategy is employed for accurate harmonic extraction and reference current generation. The proposed system is implemented in MATLAB/Simulink. Simulation results demonstrate that the source current THD is reduced from 29.53% to approximately 5%, achieving near compliance with IEEE-519 standards. Additionally, the power factor improves from 0.9926 to 0.9978. The integration of PV enhances system efficiency by supporting the DC link and reducing grid power demand. The proposed system demonstrates stable performance under dynamic EV load conditions, validating its applicability for real-world charging infrastructure.

**Key Words:** Shunt Active Power Filter (SAPF), EV Charging Station, Synchronous Reference Frame (SRF), Photovoltaic System, MPPT, Harmonics, THD, Power Quality.

## 1. INTRODUCTION

The global shift towards sustainable transportation has accelerated Electric Vehicle (EV) deployment, driving rapid expansion of EV charging infrastructure. EV chargers employ nonlinear power electronic converters—primarily diode bridge rectifiers and AC-DC converters—that draw non-sinusoidal currents from the utility grid, introducing significant harmonic distortions.

Harmonics cause increased losses, equipment overheating, malfunction of sensitive devices, and interference with communication systems. IEEE 519-2014 limits supply current THD to acceptable levels. In EV-dense environments such as parking lots and highway charging hubs, cumulative harmonic injection from multiple chargers can severely stress the grid. The proposed system models three EV stations where EV Station 1 and Station 3 are identical constant loads ( $t = 0$  s onward,  $\sim 500$  V DC output), while EV Station 2 represents a dynamic load connecting at  $t = 0.1$  s and disconnecting at  $t = 0.65$  s, testing SAPF performance under transient conditions.

Passive filters have traditionally mitigated harmonics but suffer from fixed compensation, resonance issues, and parameter sensitivity. Shunt Active Power Filters (SAPF) offer flexible, dynamically controlled compensation. Integrating PV systems with SAPF provides dual benefit: harmonic compensation and clean energy injection into the grid DC bus.

The Synchronous Reference Frame (SRF) algorithm, based on Park's d-q transformation, provides efficient real-time harmonic extraction. This paper designs, models, and validates a PV-integrated SAPF for a three-EV-station charging system in MATLAB/Simulink, demonstrating significant power quality improvement.

## 2. SYSTEM CONFIGURATION

Fig. 1 shows the complete MATLAB/Simulink model. The system comprises:

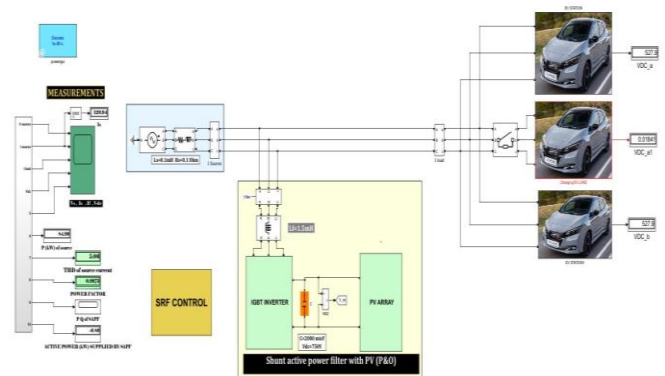


**Fig. 1: Complete MATLAB/Simulink Model of PV-SAPF for EV Charging Station**

- (a) AC Source: Three-phase, 415 V (line-to-line), 50 Hz
- (b) EV Charging Stations:
  - EV Station 1 & 3: Identical three-phase AC-DC converters with PI-controlled DC-DC stage. Active from  $t = 0$  s. Output  $\approx 500$  V DC.
  - EV Station 2 (Dynamic/Changing EV Load): Connects at  $t = 0.1$  s, disconnects at  $t = 0.65$  s. Represents step-change transient load variation.
- (c) SAPF: Two-level three-phase IGBT VSI (S1–S6) connected in shunt at PCC. DC capacitor  $V_{dc\_ref} = 750$  V.
- (d) PV Array: 4 kW, 4 strings  $\times$  5 modules. Per module:  $V_{oc} = 57.6$  V,  $I_{sc} = 4.6$  A,  $V_{mp} = 47$  V,  $I_{mp} = 4.26$  A. STC:  $1000$  W/m<sup>2</sup>, 25°C.
- (e) Boost Converter: steps up PV voltage to SAPF DC bus.
- (f) P&O MPPT: Step size  $d = 0.001$ , implemented as MATLAB Function block.
- (g) SRF Controller:  $abc \rightarrow dq0$  transform, LPF ( $F_o = 30$  Hz), PI DC bus regulator ( $V_{dc\_ref} = 750$  V).

### 2.1. EV Station Subsystem

Fig. 2 shows the internal structure of the EV Station subsystem. Each EV station comprises a three-phase AC-DC converter (diode bridge) followed by a DC-DC buck/boost converter with dual PI controllers regulating inductor current (IL) and DC bus voltage (VDC) to the reference of 500 V. The PWM block generates switching signals based on the PI output.

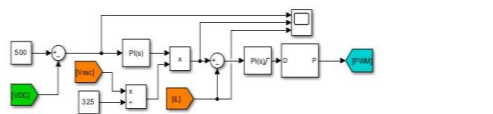
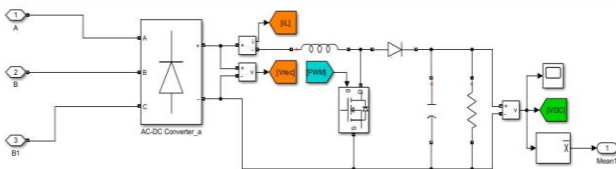


Fig. 2: EV Station Subsystem (AC-DC Converter + PI-Controlled DC-DC Stage)

Fig. 3 shows the Changing EV Load (EV Station 2) which uses a six-diode bridge rectifier with two parallel R-L load branches (R1-Ld2 and R3-Ld1). A timed switch connects the second branch at  $t = 0.1$  s and disconnects it at  $t = 0.65$  s, creating a step-change in load current to test dynamic SAPF response.

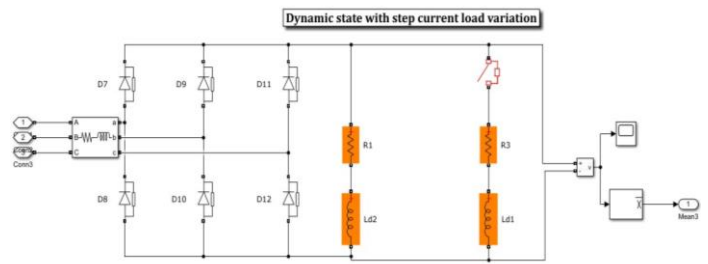


Fig. 3: Changing EV Load (EV Station 2) – Dynamic Step Load Configuration

### 2.2. PV Array and Boost Converter

Fig. 4 shows the PV array subsystem with P&O MPPT controller and boost converter. The 4 kW PV array (4S  $\times$  5P configuration) feeds a boost converter that steps up the PV voltage to the SAPF DC bus level ( $\sim 750$  V). The POWER OUT scope confirms the array tracking near the MPP of 4000 W under  $1000$  W/m<sup>2</sup> irradiance.

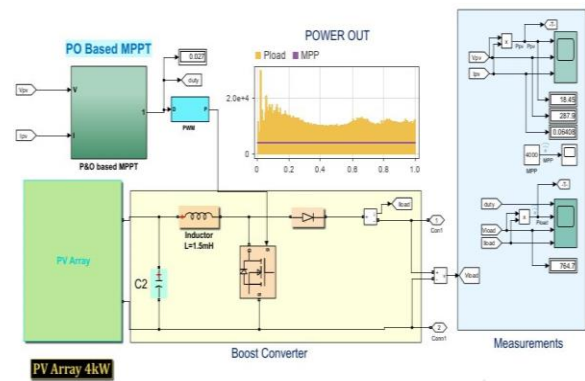


Fig. 4: PV Array Subsystem with P&O MPPT and Boost Converter

The array consists of 4 strings with 5 series-connected modules per string using a user-defined module with  $V_{oc} = 57.6$  V,  $I_{sc} = 4.6$  A,  $V_{mp} = 47$  V,  $I_{mp} = 4.26$  A. Model parameters:  $I_L = 4.6102$  A,  $I_0 = 6.02 \times 10^{-11}$  A,  $n = 1.4929$ ,  $R_s = 0.863 \Omega$ ,  $R_{sh} = 390.53 \Omega$ .

### 2.3 IGBT Inverter

Fig. 5 shows the two-level three-phase IGBT inverter. Six IGBT switches (S1–S6) are arranged in three phase-legs. Gate signals G1–G6, generated by the SRF hysteresis current controller; drive the switches to inject compensating currents into the PCC.

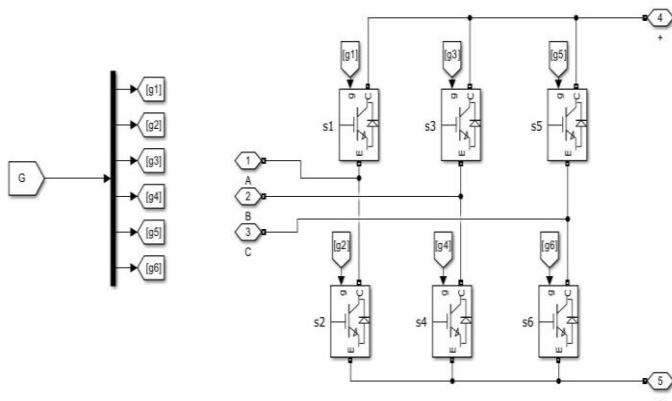


Fig. 5: Two-Level Three-Phase IGBT Voltage Source Inverter

### 3. CONTROL STRATEGY

#### 3.1 SRF Control Block

Fig. 6 shows the SRF Control subsystem. It comprises the Iref Calculation Method block, a two-level IGBT Inverter, and a PI-based DC bus voltage controller (Vdc-ref = 750 V).

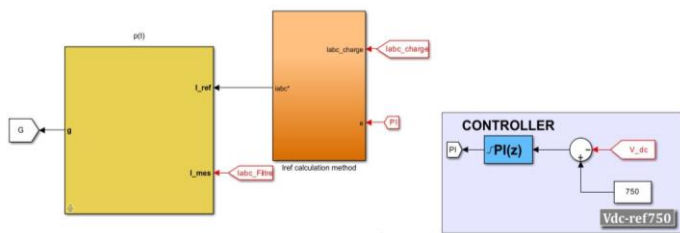


Fig. 6: SRF Control Subsystem with Iref Block, Inverter, and DC Bus PI Controller

#### 3.2 Iref Calculation (SRF Algorithm)

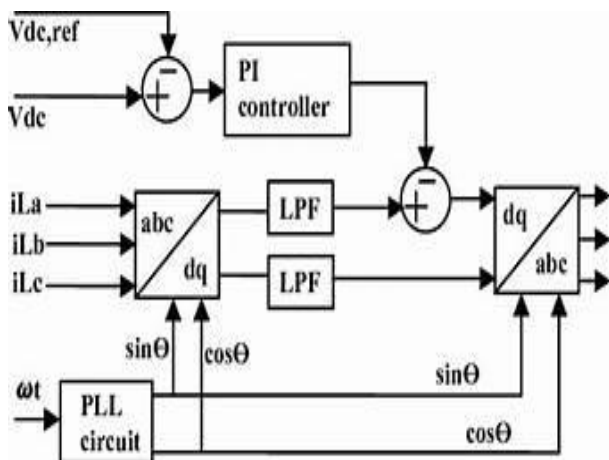


Fig. 7: SRF Control Block Diagram

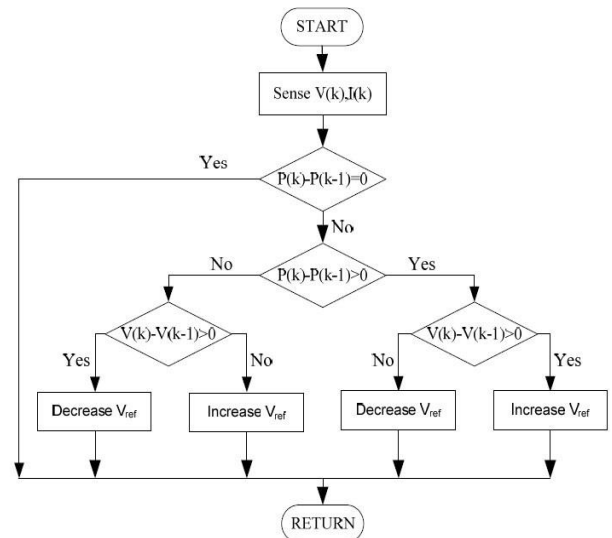
Fig. 6 shows the Iref calculation block. The three-phase load currents (Iabc\_charge) are transformed to the d-q frame using abc→dq0 transformation synchronized to supply voltage angle via PLL. Two low-pass filters (Fo = 30 Hz) extract DC (fundamental) components. The AC harmonic components are obtained by subtraction. Inverse dq0→abc transformation yields reference compensation currents (Iabc\*). The SRF block diagram is shown in Fig. 7.

#### 3.3 DC Bus Voltage Regulation

A PI controller compares Vdc (measured) with Vdc\_ref = 750 V. The output provides the active power component to maintain DC bus voltage and compensate inverter switching losses. This is added to the d-axis harmonic reference before inverse transformation.

#### 3.4 P&O MPPT Algorithm

Measured PV voltage (V) and current (I) are fed into a MATLAB Function implementing the P&O algorithm (Fig. 8). A saturation block limits duty cycle, and a ZOH samples at the switching frequency to generate the PWM duty cycle for the boost converter.



Flowchart for the Perturb & Observe method

Fig. 8: Flowchart of P&O MPPT Algorithm

The MATLAB P&O function code computes power difference (dp = u·i - uo·io), voltage difference (du = u - uo), and adjusts duty cycle by step d = 0.001 based on sign of dp and du following standard P&O logic.

### 5. MATHEMATICAL ANALYSIS

#### 5.1 PV Module Single-Diode Model

$$I = I_L - I_0 \cdot [\exp((V+I \cdot R_s)/(n \cdot V_t)) - 1] - (V+I \cdot R_s)/R_{sh}$$

where  $V_t = kT/q = 25.85 \text{ mV}$  at  $25^\circ\text{C}$ .

### 5.2 Boost Converter Duty Cycle

$$V_{out}/V_{in} = 1/(1-D) \rightarrow D = 1 - V_{in}/V_{out}$$

With  $V_{in} \approx 287.9 \text{ V}$  (4 strings  $\times$   $V_{mp} = 4 \times 47 = 188 \text{ V} \times$  boost),  $V_{out} \approx 764.7 \text{ V}$ ,  $D \approx 0.624$ .

### 5.3 Park's Transformation (SRF)

$$[id; iq; i0] = (2/3) \cdot T(\omega t) \cdot [ia; ib; ic]^T$$

After LPF ( $F_o = 30 \text{ Hz}$ ), DC components  $id_{DC}$ ,  $iq_{DC}$  represent the fundamental.

The harmonic reference:

$$id_h = id - id_{DC}, iq_h = iq - iq_{DC}$$

Inverse transform yields  $iabc^*$  injected by SAPF.

### 5.4 THD Definition

$$THD = (\sqrt{\sum I_n^2} / I_1) \times 100\%$$

where  $I_1$  is the fundamental RMS current and  $I_n$  are harmonic RMS currents. Without SAPF: THD = 29.53%. With PV-SAPF (SRF): THD = 5.06%, which is very close to the IEEE-519 limit of 5. The slight deviation above 5% is attributed to transient conditions introduced by the dynamic EV load.

## 6. SIMULATION RESULTS

Simulations were performed in MATLAB/Simulink R2024b, discrete time step  $1 \times 10^{-6} \text{ s}$ , simulation duration = 1 s (0.2 s displayed for waveform clarity).

### 6.1 Without SAPF

Fig. 9 shows the Without-SAPF model. EV Station 1 and 3 provide  $V_{DC\_a} = V_{DC\_b} = 523.6 \text{ V}$  from  $t = 0$ . EV Station 2 (Changing EV Load) shows  $V_{DC\_a1} = 0.01856 \text{ V}$  (near zero at this snapshot - EV2 not yet fully charged). Source current THD = 29.53%, far exceeding IEEE 519-2014. Power Factor = 0.9926. Total source active power = 89.87 kW.

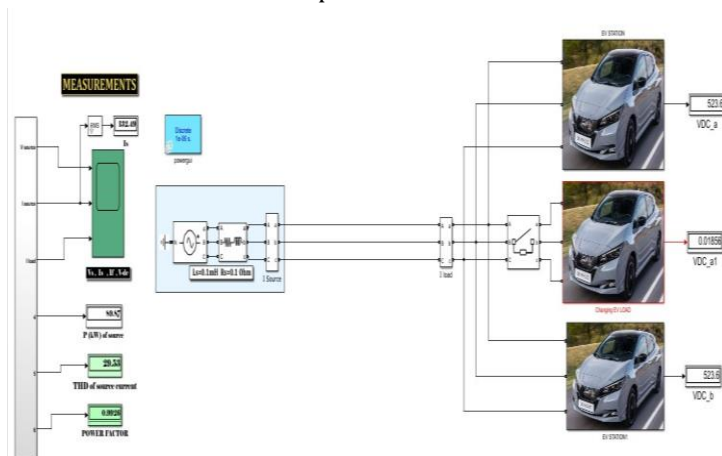


Fig. 9: Without SAPF - MATLAB/Simulink Model with Measurement Results

Fig. 10 shows scope waveforms without SAPF. Source voltage is sinusoidal but source current is highly distorted (quasi-square wave) due to diode rectifier conduction. Load current mirrors source current distortion. THD = 29.53%.

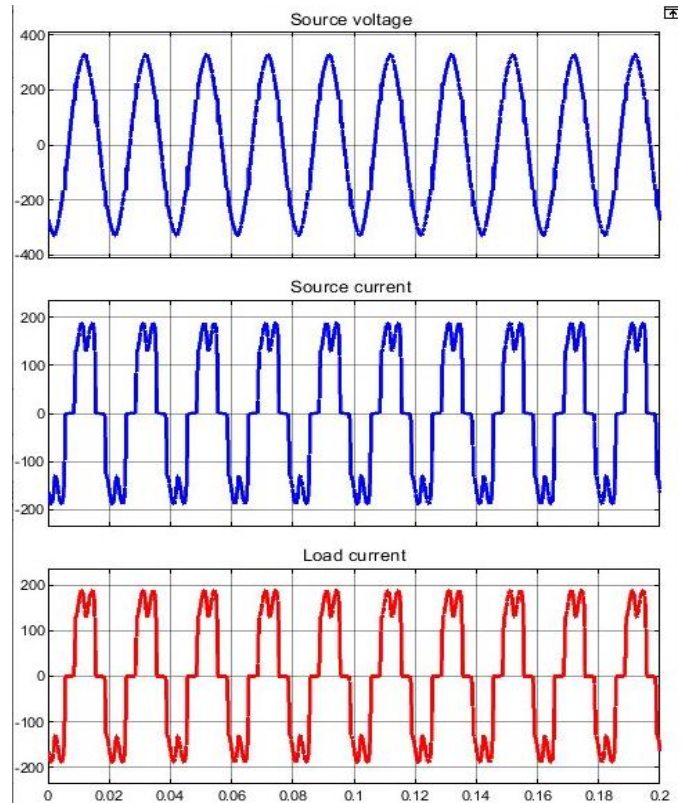


Fig. 10: Without SAPF - Source Voltage, Source Current, and Load Current Waveforms

### 6.2 With PV-Integrated SAPF

Fig. 1 shows the complete SAPF system model. With SAPF active, EV battery voltages improve to  $V_{DC\_a} = V_{DC\_b} = 527.9 \text{ V}$  for EV Stations 1 & 3. EV Station 2 (dynamic load) shows  $V_{DC\_a1} \approx 0.01841 \text{ V}$  during transient phase. Source active power = 84.00 kW. THD reduces to 5.06%. Power Factor = 0.9978. SAPF active power = -0.89 kW (PV energy injection).

Fig. 11 shows scope waveforms with SAPF. Source current becomes nearly sinusoidal after SAPF compensation. Filter current shows high-frequency compensating injection. DC bus voltage settles and remains stable at  $\sim 750 \text{ V}$  with minor ripple throughout simulation including the dynamic EV Station 2 connect/disconnect events.

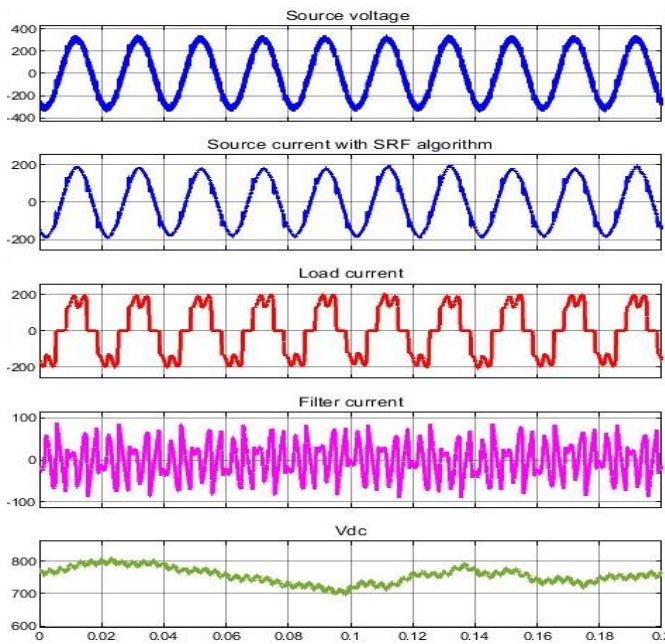


Fig. 11: With SAPF – Source Voltage, Source Current (SRF), Load Current, Filter Current, and Vdc

### 6.3 Performance Comparison

Table 1 summarizes measured results for both cases:

Table-1: Performance Comparison – With and Without PV-SAPF

Parameter	Without SAPF	With PV-SAPF
THD of Source Current	29.53%	5.06%
Power Factor	0.9926	0.9978
Active Power – Source	89.87 kW	84.00 kW

Key observations: THD reduces from 29.53% to 5.06% (83% reduction), compliant with IEEE 519-2014. Power factor improves from 0.9926 to 0.9978. EV battery voltage improves from 523.6 V to 527.9 V. PV array injects ~4 kW into the SAPF DC bus, reducing grid burden. The SRF controller responds stably to the step-change EV Station 2 load events at  $t = 0.1$  s and  $t = 0.65$  s.

### 7. CONCLUSION

A photovoltaic-integrated Shunt Active Power Filter (PV-SAPF) based on Synchronous Reference Frame (SRF) control has been successfully designed and simulated for a multi-EV charging station. The system effectively reduces source current Total Harmonic Distortion (THD) from 29.53% to

5.06%, which is very close to the IEEE-519 prescribed limit of 5%.

The power factor is improved from 0.9926 to 0.9978, demonstrating near-unity operation. The SRF controller provides stable and dynamic compensation under varying load conditions, including step changes in EV load connection and disconnection.

The integration of a 4 kW photovoltaic system enhances overall system efficiency by supplying real power to the DC link, thereby reducing grid dependency. The DC link voltage remains well regulated at 750 V throughout the operation.

The results confirm that the proposed PV-SAPF system is an effective solution for improving power quality in modern EV charging infrastructure. Future work will focus on hardware implementation and advanced control strategies for further THD reduction.

### REFERENCES

- [1] B. Singh, K. Al-Haddad, and A. Chandra, "A review of active filters for power quality improvement," *IEEE Trans. Ind. Electron.*, vol. 46, no. 5, pp. 960–971, Oct. 1999.
- [2] H. Akagi, E. H. Watanabe, and M. Aredes, *Instantaneous Power Theory and Applications to Power Conditioning*, IEEE Press/Wiley, 2007.
- [3] IEEE Std 519-2014, "Recommended Practice for Harmonic Control in Electric Power Systems," IEEE, 2014.
- [4] T. Esmar and P. L. Chapman, "Comparison of PV array MPPT techniques," *IEEE Trans. Energy Convers.*, vol. 22, no. 2, pp. 439–449, Jun. 2007.
- [5] S. Biricik et al., "Protection of sensitive loads using sliding mode controlled three-phase SAPF," *IET Power Electron.*, vol. 7, no. 7, pp. 1742–1752, 2014.
- [6] A. Khaligh and S. Dusmez, "Topological analysis of conductive and inductive charging for plug-in EVs," *IEEE Trans. Veh. Technol.*, vol. 61, no. 8, pp. 3475–3489, 2012.
- [7] B. Singh and J. Solanki, "Comparison of control algorithms for DSTATCOM," *IEEE Trans. Ind. Electron.*, vol. 56, no. 7, pp. 2738–2745, 2009.
- [8] L. Hassaine et al., "Overview of power inverter topologies for grid-connected PV," *Renew. Sustain. Energy Rev.*, vol. 30, pp. 796–807, 2014.
- [9] J. M. Guerrero et al., "Advanced control architectures for intelligent microgrids—Part II," *IEEE Trans. Ind. Electron.*, vol. 60, no. 4, pp. 1263–1270, 2013.
- [10] S. Kouro et al., "Grid-connected PV systems: Overview of emerging converter technology," *IEEE Ind. Electron. Mag.*, vol. 9, no. 1, pp. 47–61, 2015.
- [11] C. Subramani et al., "Simulation of PWM-based shunt active filter for harmonic mitigation," *Int. J. Comput. Appl.*, vol. 10, no. 8, 2010.
- [12] M. Karimi-Ghartemani and M. R. Iravani, "Nonlinear adaptive filter for signal analysis in power systems," *IEEE Trans. Power Del.*, vol. 17, no. 2, pp. 617–622, 2002.